C. R. Physique 20 (2019) 449–460

Contents lists available at ScienceDirect

Comptes Rendus Physique

www.sciencedirect.com

Fourier and the science of today / *Fourier et la science d'aujourd'hui*

Synchrosqueezing transforms: From low- to high-frequency modulations and perspectives

La transformée synchrosqueezée, adaptation aux signaux fortement modulés et perspectives

Sylvain Meignen [a,*], Thomas Oberlin [b], Duong-Hung Pham [c]

[a] *Laboratoire LJK, bâtiment IMAG, Université Grenoble Alpes, 700, avenue Centrale, Campus de Saint-Martin-d'Hères, 38401 Domaine universitaire de Saint-Martin-d'Hères, France*
[b] *IRIT, Toulouse INP – ENSEEIHT, 2, rue Charles-Camichel, BP 7122, 31071 Toulouse cedex 7, France*
[c] *ICube, UMR 7357, Laboratoire des sciences de l'ingènieur, de l'informatique et de l'imagerie, 300, bd Sébastien-Brant, CS 10413, 67412 Illkirch cedex, France*

ARTICLE INFO

Article history:
Available online 11 July 2019

Keywords:
Time-frequency analysis
Multicomponent signals
Reassignment techniques

Mots-clés :
Analyse temps-fréquence
Signaux multicomposantes
Techniques de réallocation

ABSTRACT

The general aim of this paper is to introduce the concept of synchrosqueezing transforms (SSTs) that was developed to sharpen linear time–frequency representations (TFRs), like the short-time Fourier or the continuous wavelet transforms, in such a way that the sharpened transforms remain invertible. This property is of paramount importance when one seeks to recover the modes of a multicomponent signal (MCS), corresponding to the superimposition of AM/FM modes, a model often used in many practical situations. After having recalled the basic principles of SST and explained why, when applied to an MCS, it works well only when the modes making up the signal are slightly modulated, we focus on how to circumvent this limitation. We then give illustrations in practical situations either associated with gravitational wave signals or modes with fast oscillating frequencies and discuss how SST can be used in conjunction with a demodulation operator, extending existing results in that matter. Finally, we list a series of different perspectives showing the interest of SST for the signal processing community.

RÉSUMÉ

Dans cet article, nous présentons le principe de la transformée synchrosqueezée (SST) développée pour améliorer, en utilisant des techniques de réallocation, la qualité des représentations linéaires temps–fréquence, comme les transformées de Fourier à court terme ou en ondelettes. Les transformées réallouées demeurent inversibles, ce qui est fondamental pour l'étude des signaux multicomposantes (MCS), i.e. la superposition de modes modulés à la fois en amplitude et en fréquence, utilisés comme modèle dans de nombreuses applications. Cependant, la SST, dans sa formulation initiale, n'est pas adaptée aux signaux composés de modes fortement modulés, et des améliorations, que nous présentons ici, ont récemment été proposées pour pallier ce défaut. Pour illustrer

* Corresponding author.
E-mail addresses: sylvain.meignen@univ-grenoble-alpes.fr (S. Meignen), thomas.oberlin@enseeiht.fr (T. Oberlin), dhpham@unistra.fr (D.-H. Pham).

https://doi.org/10.1016/j.crhy.2019.07.001

ces nouveaux développements, nous étudierons le cas des ondes gravitationnelles et des modes à phase oscillante. Dans un second temps, nous montrerons comment utiliser conjointement la SST et la démodulation pour améliorer la reconstruction des modes d'un MCS, et terminerons en évoquant différentes perspectives actuelles autour de la SST.

1. Introduction

Since its foundation, the field of signal and image processing has always made intensive use of frequency representations, and today, Fourier analysis, or more generally speaking harmonic analysis, is the fundamental tool to analyze or process signals or images [1]. Many reasons can explain why the use of Fourier theory is so widespread inside the signal processing community. First, the notion of *frequency* is essential to describe oscillatory signals, as for instance sounds. Second, the Fourier transform (FT) is intrinsically related to linear time-invariant filters often used to model the response of physical systems or sensors. Last, when considering random measurements, FT allows us to easily model or simulate stationary Gaussian random fields. In this paper, we will particularly focus on the first point, that is to design a frequency analysis framework, but adapted to *non-stationary* signals.

Indeed, the main limitation of FT is that it does not locate in time the frequency information computed on a given signal, while most signals from the physical world are intrinsically non-stationary, in the sense that their frequencies vary along time. Analyzing or processing these signals efficiently thus requires the use of *local* transformations, called *time–frequency representations* (TFRs), among which the most popular is probably the *short-time Fourier transform* (STFT), which basically windows the signal around the time of interest before applying FT. Note that the window cannot be of arbitrary length since, according to the Heisenberg–Gabor uncertainty principle [1], a small temporal window (associated with a good time localization) leads to a bad frequency resolution, and vice-versa. Another popular TFR is the *continuous wavelet transform* (CWT) [2], which shares many properties with STFT, but is based on a different frequency resolution. While both transforms are invertible and allow one to process non-stationary signals, they suffer from a strong limitation, that is, the time–frequency (TF) resolution is constrained by the choice of window or wavelet, limiting both the adaptivity of the proposed analysis and the readability of the TFR.

Many works in the past decades have tackled this limitation, by using, for instance, quadratic TFRs, e.g., Wigner–Ville distributions [3], which are not constrained by the uncertainty principle, but exhibit strong interference hampering the representation and are not invertible. Another attempt, called the *reassignment method* (RM), dating back to the work by Kodera et al. [4] in the 1970s and then further developed in [5], essentially proposed a means of improving the TFR readability. Unfortunately, the reassigned representation was also no longer invertible. This in particular means that, when applied to the TFR of a multicomponent signal (MCS) made of AM/FM modes, RM does not allow for an easy retrieval of the components of the MCS. Other works, like the Empirical Mode Decomposition (EMD) [6], precisely focused on this latter aspect and consists of a simple algorithm to adaptively decompose an MCS into modulated AM/FM waves. While it proved to be interesting in many practical applications, it lacks mathematical foundations and behaves like a filter bank resulting in mode mixing [7]. To partially overcome these drawbacks, recent works tried to mimic EMD but using a more stable framework, either based on wavelet transforms [8] or convex optimization [9,10].

Synchrosqueezing transform (SST) is yet another approach whose initial goal was to improve the readability of the TFR given by CWT [11] using a reassignment procedure, in such a way that the reassigned transform was still invertible. This has the nice consequence that the retrieval of the modes of an MCS is then possible from the reassigned transform [12], which is of great practical interest. Indeed, real-life signals are often modeled by means of MCS, found in a wide range of applications such as audio recordings, structural stability [13,14], or physiological signals [15,16]. Because, in these instances, the modes are essentially AM/FM, TFRs are well adapted to represent such non-stationary signals and SST proved to be an efficient technique to obtain improved TFRs while allowing for mode retrieval.

SST has recently been extended in many ways: it was adapted to STFT, known as *STFT-based SST* (FSST) in [17], for which mathematical analyses are available in [18–20], a bidimensional extension was proposed by means of the monogenic wavelet transform [21,22], and a multivariate extension adapted to quasi-circular modulated signals was also proposed in the context of brain electrical recordings [23]. In another direction, a multi-taper approach was proposed to increase the resolution and the robustness of SST, as in the *ConceFT* method [24], and the case of non-harmonic waves investigated in [25]. In spite of all these advances, one major problem associated with SST in its original formulation is that it cannot deal with MCSs containing modes with strong frequency modulation, which are very common in many fields of practical interest, as for instance radar [26], speech processing [27], gravitational waves [28,29], or in the analysis of otoacoustic emissions [30]. In this regard, an adaption of FSST to better handle that type of signals, known as the *second-order synchrosqueezing transform* (FSST2), was introduced in [20], and its theoretical foundations settled in [31]. Such a new transform was also used in a demodulation algorithm [32] and extended to better deal with modes with fast oscillating phase [33].

In this paper, we will briefly recall some useful definitions in Section 2, and then those of SST in the STFT and CWT settings in Section 3, before putting the emphasis on the different behaviors of these two transforms. Then, we will present an overview of recent developments on SST, including those on higher-order SST [31,33] and on the design of the demodulation algorithm in the SST context [32]. Then, we will give details on practical implementation, an aspect often left apart in the literature.

2. Background

Consider a signal $f \in L^1(\mathbb{R})$, its *Fourier transform* corresponds to:

$$\widehat{f}(\xi) = \mathcal{F}\{f\}(\xi) = \int_{\mathbb{R}} f(t)\, \mathrm{e}^{-2\pi \mathrm{i}\xi t}\, \mathrm{d}t \tag{1}$$

and its *short-time Fourier transform* (STFT) is defined using any sliding window $g \in L^\infty(\mathbb{R})$ by:

$$V_f^g(t,\xi) = \int_{\mathbb{R}} f(\tau) g(\tau - t)\, \mathrm{e}^{-2\pi \mathrm{i}\xi(\tau - t)}\, \mathrm{d}\tau = \int_{\mathbb{R}} f(t+\tau) g(\tau)\, \mathrm{e}^{-2\pi \mathrm{i}\xi\tau}\, \mathrm{d}\tau \tag{2}$$

If f, $\hat{f}$, g and $\hat{g}$ are all in $L^1(\mathbb{R})$, f can be reconstructed from its STFT as soon as g is non-zero at 0:

$$f(t) = \frac{1}{\overline{g(0)}} \int_{\mathbb{R}} V_f^g(t,\xi)\, \mathrm{d}\xi \tag{3}$$

where $\overline{Z}$ denotes the complex conjugate of Z.

In this paper, we will intensively study multicomponent signals (MCSs) defined as a superimposition of AM/FM components or modes:

$$f(t) = \sum_{k=1}^{K} f_k(t) \quad \text{with} \quad f_k(t) = A_k(t)\, \mathrm{e}^{2\pi \mathrm{i}\phi_k(t)} \tag{4}$$

for some finite $K \in \mathbb{N}$, $A_k(t)$ and $\phi_k'(t)$ being respectively the instantaneous amplitude (IA) and frequency (IF) f_k satisfying: $A_k(t) > 0$, $\phi_k'(t) > 0$ and $\phi_{k+1}'(t) > \phi_k'(t)$ for all t. Such a signal admits an ideal TF (ITF) representation defined as:

$$\mathrm{TI}_f(t,\omega) = \sum_{k=1}^{K} A_k(t) \delta\left(\omega - \phi_k'(t)\right) \tag{5}$$

where δ denotes the Dirac distribution. In practice, the IF of the modes cannot be recovered by estimating the IF of f as is done in the theory of analytical signals, and to locate the modes in the TF plane is essential before computing the IF of each mode: this is one of the goals of SST, whose construction is recalled hereafter.

3. The synchrosqueezing transform

SST pursues two main objectives: first to sharpen a given linear TFR, and then, when applied to an MCS, to separate and retrieve the modes. The transform is based on an estimation, from the TFR, of the IF of each mode, then used to sharpen the energy of the representation around so-called *ridges*, approximating the curves $(t, \phi_k'(t))$. SST operating on a linear TFR, e.g., STFT or CWT, also allows for mode retrieval exploiting the synthesis formula (3), as will be recalled later. SST was first introduced in [11,12] in the CWT setting, and then adapted to STFT in [18–20]. In this paper, we mainly focus on STFT-based SST, and we will therefore only mention, when necessary, the one based on CWT.

3.1. STFT-based synchrosqueezing transform

STFT based synchrosqueezing (denoted by FSST in the sequel) is based on the definition of the *local instantaneous frequency estimate* $\widehat{\omega}_f$ [5]:

$$\widehat{\omega}_f(t,\xi) = \frac{\partial \arg V_f^g(t,\xi)}{\partial t} = \Re\left\{ \frac{1}{2\pi \mathrm{i}} \frac{\partial_t V_f^g(t,\xi)}{V_f^g(t,\xi)} \right\}, \text{ wherever } V_f^g(t,\xi) \neq 0 \tag{6}$$

The FSST of f with threshold γ is then obtained by moving any coefficient $V_f^g(t,\xi)$ with magnitude larger than γ to location $(t, \widehat{\omega}_f(t,\xi))$. This can be formally written as:

$$T_f^{\gamma}(t,\omega) = \int\limits_{|V_f^g(t,\xi)|>\gamma} V_f^g(t,\xi)\delta(\omega - \widehat{\omega}_f(t,\xi))\,\mathrm{d}\xi \tag{7}$$

Any mode f_k can then be reconstructed by summing FSST coefficients around the kth ridge, which amounts to modifying the synthesis formula (3) to select only the coefficients related to the kth mode, namely:

$$f_k(t) \approx \frac{1}{g(0)} \int\limits_{|\omega-\varphi_k(t)|<d} T_f^{\gamma}(t,\omega)\,\mathrm{d}\omega \tag{8}$$

where φ_k is an estimate of ϕ_k', and parameter d is used to compensate for errors in IF estimation; it should be kept small enough to avoid mode-mixing, and its influence will be discussed later.

3.2. Wavelet-based synchrosqueezing transform

Let ψ be a wavelet; we define, at time t and scale $a > 0$, the *continuous wavelet transform* (CWT) of f by:

$$W_f^{\psi}(t,a) = \frac{1}{a}\int\limits_{\mathbb{R}} f(\tau)\overline{\psi\left(\frac{\tau - t}{a}\right)}\,\mathrm{d}\tau \tag{9}$$

If f and $\hat{f}$ are in $L^1(\mathbb{R})$ and f or ψ is analytic (which means, not containing any negative frequency), and assuming that $C_{\psi}' = \int_0^{+\infty} \overline{\widehat{\psi}(\xi)}\frac{\mathrm{d}\xi}{\xi} < \infty$, the wavelet-based SST (WSST) local instantaneous frequency estimate is defined by:

$$\widehat{\omega}_f(t,a) = \Re\left\{\frac{1}{2\pi\mathrm{i}}\frac{\partial_t W_f^{\psi}(t,a)}{W_f^{\psi}(t,a)}\right\} \tag{10}$$

WSST then consists in vertically moving the coefficients according to the map $(t,a) \mapsto (t, \widehat{\omega}_f(t,a))$:

$$S_f^{\gamma}(t,\omega) = \int\limits_{|W_f^{\psi}(t,a)|>\gamma} W_f^{\psi}(t,a)\delta\left(\omega - \widehat{\omega}_f(t,a)\right)\frac{\mathrm{d}a}{a} \tag{11}$$

The kth mode can then be approximately reconstructed by integrating $S_f^{\gamma}(t,\omega)$ along the frequency axis as follows:

$$f_k(t) \approx \frac{1}{C_{\psi}'} \int\limits_{|\omega-\varphi_k(t)|<d} S_f^{\gamma}(t,\omega)\,\mathrm{d}\omega \tag{12}$$

3.3. Approximation results for FSST and WSST

As pointed out in the introduction, the success of SST is partly due to the nice theoretical results pioneered in [12], of which we here give a flavor (referring the reader to [12] and [20] for details on WSST and FSST, respectively). These results consider MCSs as in equation (4), assuming that:

(i) Each f_k is a perturbation of a pure wave, i.e. its IA A_k and IF ϕ_k' are *slow varying*.
(ii) The different modes are *separated* in the TF plane, i.e. for each time t $\phi_k'(t)$ for $k = 1 \cdots K$ are significantly different.

Even though FSST and WSST are very similar in nature, they behave well on different types of MCSs. Indeed, while both techniques enable a perfect representation and reconstruction of purely harmonic modes [12,20], this is no longer the case when the modes are modulated.

The main difference between the two transforms is related to the frequency resolution: STFT has a fixed frequency resolution, whereas the resolution of CWT depends on the scale (or frequency). Thus the slow variation for $A_k'(t)$ and $\phi_k''(t)$ and separation assumptions for the IF of the modes in the CWT setting are relative to the IF ϕ_k', i.e. $|A_k'(t)|$, $|\phi_k''(t)| \ll \phi_k'(t)$ and $\frac{\phi_{k+1}'(t)-\phi_k'(t)}{\phi_{k+1}'(t)+\phi_k'(t)} \geq \Delta$ (Δ being the frequency bandwidth of the wavelet), respectively, whereas in the STFT setting these are constant all over the TF plane, i.e. $|A_k'(t)|$, $|\phi_k''(t)| \ll 1$ and $\phi_{k+1}'(t) - \phi_k'(t) \geq 2\Delta$ (Δ being the frequency bandwidth of the window g), respectively. As a first simple example to illustrate these differences, one may consider a signal made of two parallel linear chirps (i.e. with linear IFs), for which the separation assumption is more stringent at high than at low frequencies when using WSST because of the division by $\phi_2'(t) + \phi_1'(t)$, but such is not the case with FSST.

A second example is the 3-mode signal shown in Fig. 1, made of a pure harmonic wave, a linear chirp and a hyperbolic chirp (i.e. with IF satisfying $\phi''(t) = Cst\,\phi'(t)^2$). We first note that the FSST and WSST of the purely harmonic mode are very

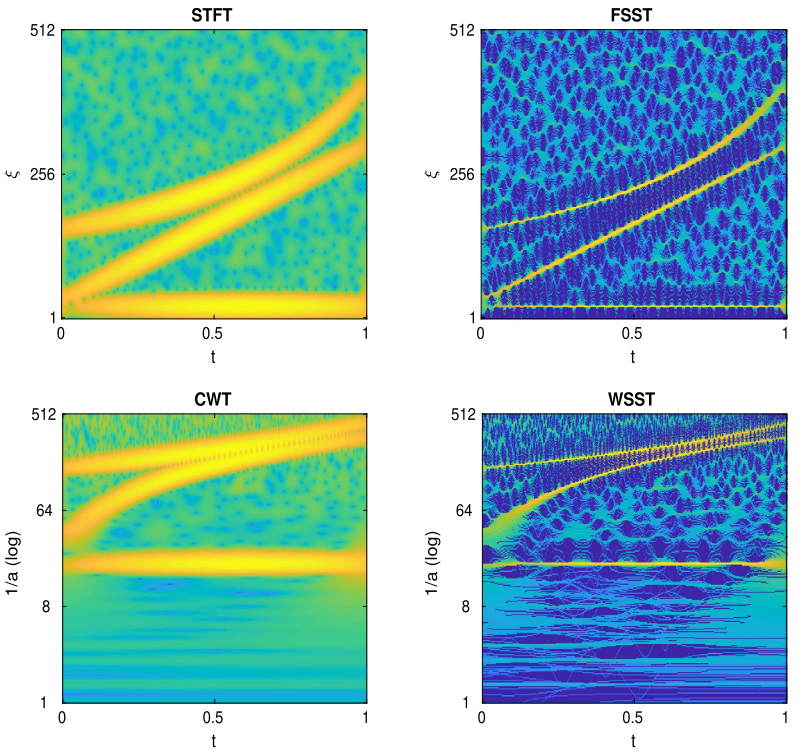

Fig. 1. Illustration of STFT, CWT, FSST and WSST on a synthetic signal.

much the same, then regarding the representation of the linear chirp, we observe that since the resolution with CWT is much better at low frequencies, the representation associated with WSST is less sharp in these instances (close to $t = 0$), and the reverse is also true, i.e. the representation is sharper when the frequency increases. On the contrary, the sharpness of the representation remains the same whatever the frequency when one considers FSST. Regarding the exponential chirp, since it is located in the high-frequency part of the TF plane, the frequency resolution with WSST is poor, resulting in a sharp representation, while for FSST the resolution being the same whatever the frequency, the representation becomes less and less sharp when the modulation increases. A last interesting point regarding the analysis of Fig. 1 is that the separation of the hyperbolic chirp from the linear one seems much simpler with FSST than with WSST, as a consequence of the fact that these modes at high frequencies are closer in the time-scale (TS) than TF planes.

4. Higher-order SST

4.1. Second order synchrosqueezing transforms

As just explained, the applicability of FSST is restricted to a class of MCSs composed of slightly perturbed purely harmonic modes. To overcome this limitation, an extension of FSST was introduced based on a more accurate IF estimate, then used to define an improved synchrosqueezing operator, called *second-order STFT-based synchrosqueezing transform* (FSST2) [34,31]. More precisely, one first defines a *second-order local modulation operator*, which is then used to compute the new IF estimate. To do so, one introduces complex reassignment operators $\tilde{\omega}_f(t,\xi) = \frac{\partial_t V_f^g(t,\xi)}{2\pi \mathrm{i} V_f^g(t,\xi)}$ and $\tilde{t}_f(t,\xi) = t - \frac{\partial_\xi V_f^g(t,\xi)}{2\pi \mathrm{i} V_f^g(t,\xi)}$, and then one defines a complex frequency modulation operator as [34]:

$$\tilde{q}_f(t,\xi) = \frac{\partial_t \tilde{\omega}_f(t,\xi)}{\partial_t \tilde{t}_f(t,\xi)} = \frac{\partial_t \left(\frac{\partial_t V_f^g(t,\xi)}{V_f^g(t,\xi)} \right)}{2\pi \mathrm{i} - \partial_t \left(\frac{\partial_\xi V_f^g(t,\xi)}{V_f^g(t,\xi)} \right)} \tag{13}$$

The second-order local modulation operator then corresponds to $\Re\left\{\tilde{q}_f(t,\xi)\right\}$, and the second order complex IF estimate of f is defined by:

$$\tilde{\omega}_f^{[2]}(t,\xi) = \begin{cases} \tilde{\omega}_f(t,\xi) + \tilde{q}_f(t,\xi)(t - \tilde{t}_f(t,\xi)) & \text{if } \partial_t \tilde{t}_f(t,\xi) \neq 0 \\ \tilde{\omega}_f(t,\xi) & \text{otherwise,} \end{cases} \tag{14}$$

and we then put $\hat{\omega}_f^{[2]}(t,\xi) = \Re\left\{\widetilde{\omega}_f^{[2]}(t,\xi)\right\}$. It was proven in [31] that $\hat{\omega}_f^{[2]}(t,\xi) = \phi'(t)$, when f is a Gaussian modulated linear chirp. It is also worth mentioning here that $\tilde{q}_f(t,\xi)$ can be computed by means of five different STFTs. Finally, FSST2 is defined by replacing $\hat{\omega}_f(t,\xi)$ by $\hat{\omega}_f^{[2]}(t,\xi)$ in (7), to obtain the so-called $T^{\gamma}_{2,f}$, and mode reconstruction is then performed by replacing T^{γ}_f by $T^{\gamma}_{2,f}$ in (8).

Similarly, complex reassignment operators $\widetilde{\omega}_f(t,a)$ and $\widetilde{\tau}_f(t,a)$ in the CWT context are respectively defined, for any (t,a) s.t. $W_f^{\psi}(t,a) \neq 0$, by:

$$\widetilde{\omega}_f(t,a) = \frac{1}{2\pi \mathrm{i}} \frac{\partial_t W_f^{\psi}(t,a)}{W_f^{\psi}(t,a)} \text{ and } \widetilde{\tau}_f(t,a) = \frac{\int_{\mathbb{R}} \tau f(\tau) \frac{1}{a} \overline{\psi(\frac{\tau - t}{a})} \,\mathrm{d}\tau}{W_f^{\psi}(t,a)} = t + a \frac{W_f^{t\psi}(t,a)}{W_f^{\psi}(t,a)} \tag{15}$$

The second-order local complex modulation operator corresponds to $\widetilde{q}_f(t,a) = \frac{\partial_t \widetilde{\omega}_f(t,a)}{\partial_t \widetilde{\tau}_f(t,a)}$ and the definition of the improved complex IF estimate associated with CWT is derived as:

$$\widetilde{\omega}_f^{[2]}(t,a) = \begin{cases} \widetilde{\omega}_f(t,a) + \widetilde{q}_f(t,a)(t - \widetilde{\tau}_f(t,a)) & \text{if } \partial_t \widetilde{\tau}_f(t,a) \neq 0 \\ \widetilde{\omega}_f(t,a) & \text{otherwise} \end{cases} \tag{16}$$

whose real part $\widehat{\omega}_f^{[2]}(t,a) = \Re\{\widetilde{\omega}_f^{[2]}(t,a)\}$ is the desired IF estimate. It was shown in [35] that $\Re\left\{\widetilde{q}_f(t,a)\right\} = \phi''(t)$ when f is a Gaussian modulated linear chirp, i.e. $f(t) = A(t)\,\mathrm{e}^{2\pi \mathrm{i}\phi(t)}$ where both $\log(A(t))$ and $\phi(t)$ are quadratic and that $\Re\{\widetilde{\omega}_f^{[2]}(t,a)\}$ is an exact estimate of $\phi'(t)$ for that kind of signals. For a more general mode with Gaussian amplitude, its IF can be estimated by $\Re\{\widetilde{\omega}_f^{[2]}(t,a)\}$. As for FSST2, $\widetilde{\omega}_f(t,a)$ and $\widetilde{q}_f(t,a)$ can be computed by means of only five CWTs. The second-order WSST (WSST2) is then defined by simply replacing $\widehat{\omega}_f(t,a)$ by $\widehat{\omega}_f^{[2]}(t,a)$ in (11):

$$S^{\gamma}_{2,f}(t,\omega) := \int\limits_{|W_f^{\psi}(t,a)| > \gamma} W_f^{\psi}(t,a) \delta\left(\omega - \widehat{\omega}_f^{[2]}(t,a)\right) \frac{\mathrm{d}a}{a} \tag{17}$$

and f_k is finally retrieved by replacing $S^{\gamma}_f(t,\omega)$ with $S^{\gamma}_{2,f}(t,\omega)$ in (12).

4.2. Higher-order synchrosqueezing transforms

Despite FSST2 definitely sharpens the TFR it is based on, it is proved to provide a truly sharp TFR only for perturbations of linear chirps with Gaussian modulated amplitudes. To handle signals containing more general types of AM/FM modes having non-negligible $\phi_k^{(n)}(t)$ for $n \geq 3$, especially those with fast oscillating phase, one defines new SST operators based on third- or higher-order approximations of both the amplitude and phase [33]. To introduce the technique, we restrict ourselves to the STFT context, but the technique presented hereafter could easily be extended to the CWT setting. Let $f(\tau) = A(\tau)\,\mathrm{e}^{2\pi \mathrm{i}\phi(\tau)}$ with $A(\tau)$ (*resp.* $\phi(\tau)$) being equal to its Lth-order (*resp.* Nth-order) Taylor expansion for τ close to t, namely:

$$\log(A(\tau)) = \sum_{k=0}^{L} \frac{[\log(A)]^{(k)}(t)}{k!} (\tau - t)^k \text{ and } \phi(\tau) = \sum_{k=0}^{N} \frac{\phi^{(k)}(t)}{k!} (\tau - t)^k \tag{18}$$

where $Z^{(k)}(t)$ denotes the kth derivative of Z evaluated at t. Such a mode, with $L \leq N$, can be written as:

$$f(\tau) = \exp\left(\sum_{k=0}^{N} \frac{1}{k!} \left([\log(A)]^{(k)}(t) + 2\pi \mathrm{i}\phi^{(k)}(t)\right)(\tau - t)^k\right) \tag{19}$$

since $[\log(A)]^{(k)}(t) = 0$ if $L + 1 \leq k \leq N$. Its corresponding STFT writes:

$$V_f^g(t,\xi) = \int\limits_{\mathbb{R}} f(\tau + t) g(\tau)\,\mathrm{e}^{-2\pi \mathrm{i}\xi\tau}\,\mathrm{d}\tau = \int\limits_{\mathbb{R}} \exp\left(\sum_{k=0}^{N} \frac{1}{k!} \left([\log(A)]^{(k)}(t) + 2\pi \mathrm{i}\phi^{(k)}(t)\right)\tau^k\right) g(\tau)\,\mathrm{e}^{-2\pi \mathrm{i}\xi\tau}\,\mathrm{d}\tau$$

By taking the partial derivative of $V_f^g(t,\xi)$ with respect to t and then dividing by $2\pi \mathrm{i} V_f^g(t,\xi)$, the local complex reassignment operator $\tilde{\omega}_f(t,\xi)$ defined in Section 4.1 can be written, when $V_f^g(t,\xi) \neq 0$, as:

$$\tilde{\omega}_f(t,\xi) = \sum_{k=1}^{N} r_k(t) \frac{V_f^{t^{k-1}g}(t,\xi)}{V_f^g(t,\xi)} = \frac{1}{2\pi \mathrm{i}} [\log(A)]'(t) + \phi'(t) + \sum_{k=2}^{N} r_k(t) \frac{V_f^{t^{k-1}g}(t,\xi)}{V_f^g(t,\xi)} \tag{20}$$

where $r_k(t) = \frac{1}{(k-1)!}\left(\frac{1}{2\pi \mathrm{i}}[\log(A)]^{(k)}(t) + \phi^{(k)}(t)\right)$. It is clear that to get an exact IF estimate for the studied signal, one needs to subtract $\Re\left\{\sum_{k=2}^{N} r_k(t)\frac{V_f^{t^{k-1}g}(t,\xi)}{V_f^g(t,\xi)}\right\}$ to $\Re\left\{\tilde{\omega}_f(t,\xi)\right\}$, which requires the calculation of $r_k(t)$ for $k = 2, \ldots, N$. For that purpose, one derives a frequency modulation operator $\tilde{q}_f^{[k,N]}(t,\xi)$, equal to $r_k(t)$ for the type of modes just introduced, and obtained by differentiating different STFTs with respect to ξ (to differentiate with respect to ξ rather than t leads to much simpler expressions). $\tilde{q}_f^{[k,N]}(t,\xi)$ for $2 \leq k \leq N$ can be derived recursively, following [33]:

$$\tilde{q}_f^{[N,N]}(t,\xi) = y_N(t,\xi) \text{ and } \tilde{q}_f^{[j,N]}(t,\xi) = y_j(t,\xi) - \sum_{k=j+1}^{N} x_{k,j}(t,\xi)\tilde{q}_f^{[k,N]}(t,\xi),\ N-1 \geq j \geq 2 \tag{21}$$

where $y_j(t,\xi)$ and $x_{k,j}(t,\xi)$ are defined as follows:

$$y_1(t,\xi) = \tilde{\omega}_f(t,\xi) \qquad \text{and } x_{k,1}(t,\xi) = \frac{V_f^{t^{k-1}g}(t,\xi)}{V_f^g(t,\xi)}, \qquad 1 \leq k \leq N,$$

$$y_j(t,\xi) = \frac{\partial_\xi y_{j-1}(t,\xi)}{\partial_\xi x_{j,j-1}(t,\xi)} \qquad \text{and } x_{k,j}(t,\xi) = \frac{\partial_\xi x_{k,j-1}(t,\xi)}{\partial_\xi x_{j,j-1}(t,\xi)}, \qquad 2 \leq j \leq N \text{ and } j \leq k \leq N$$

The definition of the Nth-order IF estimate then follows [33]:

$$\tilde{\omega}_f^{[N]}(t,\xi) = \begin{cases} \tilde{\omega}_f(t,\xi) + \sum_{k=2}^{N} \tilde{q}_f^{[k,N]}(\xi,t)\left(-x_{k,1}(t,\xi)\right), \text{ if } V_f^g(t,\xi) \neq 0, \text{ and } \partial_\xi x_{j,j-1}(t,\xi) \neq 0, 2 \leq j \leq N \\ \tilde{\omega}_f(t,\xi) \quad \text{otherwise} \end{cases}$$

The real part $\hat{\omega}_f^{[N]}(t,\xi) = \Re\{\tilde{\omega}_f^{[N]}(t,\xi)\}$ is the desired IF estimate, which is, by construction, exact for f satisfying (19). As for FSST2, the Nth-order FSST (FSSTN) is defined by replacing $\hat{\omega}_f(t,\xi)$ by $\hat{\omega}_f^{[N]}(t,\xi)$ in (7) to obtain $T_{N,f}^{\gamma}(t,\omega)$ and the modes of the MCS can be reconstructed by replacing $T_f^{\gamma}(t,\omega)$ by $T_{N,f}^{\gamma}(t,\omega)$ in (8).

4.3. Illustration

To illustrate the benefits brought by higher order FSSTs, we consider a synthetic mono-component signal defined as: $f(t) = A(t)\,\mathrm{e}^{2\pi \mathrm{i}\phi(t)}$ with $A(t) = 1 + 3t^2 + 4(1-t)^7$ and $\phi(t) = 240t - 2\exp(-2t)\sin(14\pi t)$ for $t \in [0,1]$, which corresponds to a damped-sine function signal containing very strong nonlinear sinusoidal frequency modulations and high-order polynomial amplitude modulations. Such a function is sampled at a rate $N = 1024$ Hz on $[0,1]$. The STFT of f is then computed with the L^1-normalized Gaussian window $g(t) = \sigma^{-1}\,\mathrm{e}^{-\pi\frac{t^2}{\sigma^2}}$, where σ is the optimal value determined by the Rényi entropy technique introduced in [36]. To use this optimal value for the window length parameter is crucial, since it allows for a good tradeoff between time and frequency resolutions and also a good mode retrieval performance [33]. In Fig. 2 (a) and (b), the real part of the signal f superimposed with A and its STFT modulus are respectively displayed. Then, in the second row of Fig. 2, we show close-ups of STFT and of reassigned representations given by FSSTs of the first four orders. It is clear that the higher the order of FSST the sharper the TFR, especially when the IF of the mode has a non-negligible *curvature* $\phi''(t)$.

A second illustration considers the gravitational wave signal GW151226 [37], produced by the collision of two black holes and recorded by the LIGO and Virgo Scientific Collaborations. It mainly consists of a chirp whose IF is increasing until the merging phase. This signal has been pre-processed as specified in the Gravitational Wave Open Science Center.[1] However, such pre-processing does not remove all the noise, which makes the chirp hardly distinguishable (Fig. 3 (b) (bottom)). We applied WSST2, which seems to effectively sharpen the TFR given by CWT (Fig. 3 (a)). This enabled the retrieval of the main mode, displayed in Fig. 3 (b) (top) along with the theoretically predicted gravitational signal. We can observe a good correspondence until $t = 0$, after which the signal is no longer an AM/FM mode. It is worth remarking here that the reassignment operation is directly performed on the noisy CWT and that no extra denoising procedure is needed, which demonstrates that SST is somewhat robust, even though little has been done so far to quantify this robustness.

[1] https://www.gw-openscience.org/GW151226data/LOSC_Event_tutorial_GW151226.html.

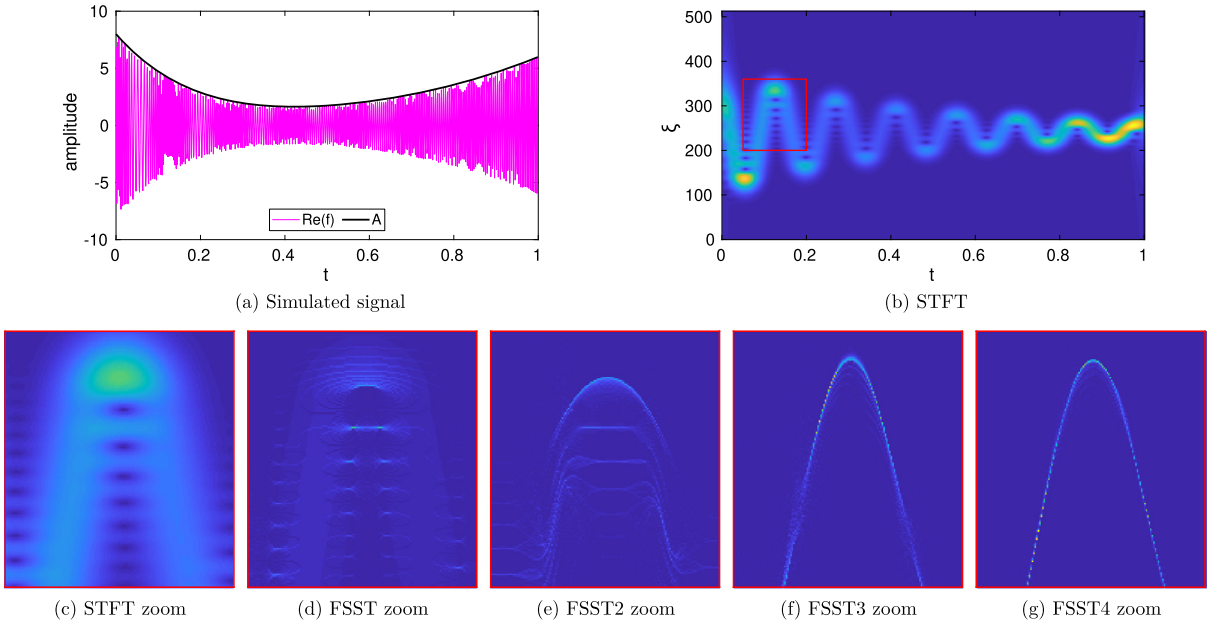

(a) Simulated signal (b) STFT

(c) STFT zoom (d) FSST zoom (e) FSST2 zoom (f) FSST3 zoom (g) FSST4 zoom

Fig. 2. Illustration of the difference between second-, third-, and fourth-order FSSTs: (a) real part of f with A superimposed; (b) modulus of the STFT of f; (c) STFT zoom of a small TF patch (delimited by a red rectangle) extracted from (b); (d) FSST zoom carried out on the STFT shown in (c); from (d) to (g), same as (d) but for FSST2, FSST3, and FSST4, respectively.

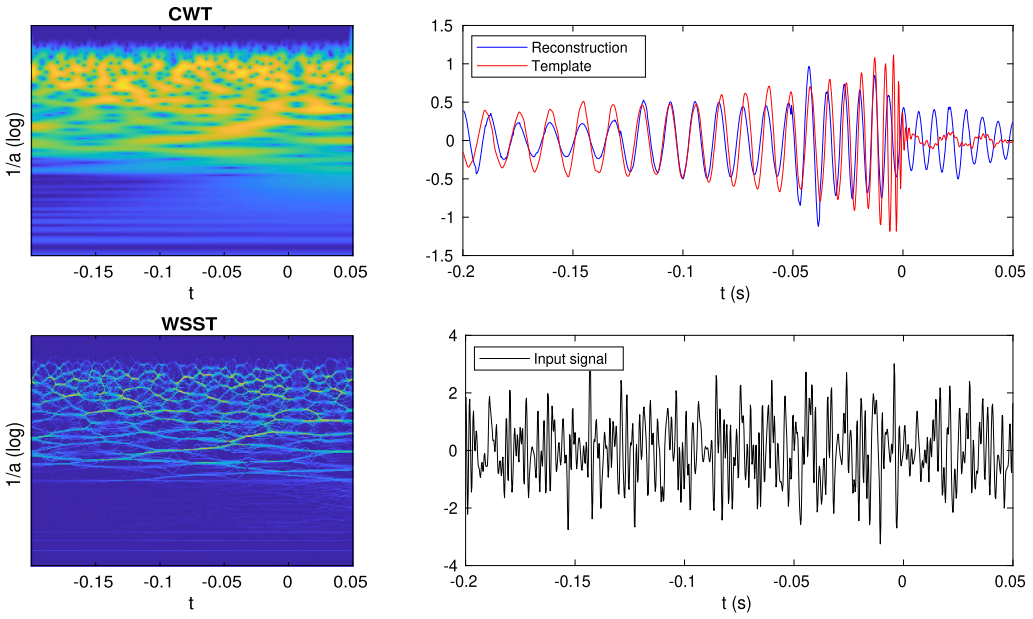

(a) (b)

Fig. 3. Illustration of the second-order WSST2 on a gravitational wave signal.

5. Practical implementation

5.1. Settings parameters

Most of the theoretical works on SST studied the continuous time and frequency settings, while in practice both time and frequency are discretized and this requires special attention. In particular and as already shown in Fig. 1, the frequency resolution directly impacts the sharpness of the reassigned transform. Furthermore, SSTs depend on two main parameters: the choice of window or wavelet defining the TFR, and the threshold γ used in the definition of the SSTs. Although there is no ideal way to determine the window length, a common practice is to consider the window (or wavelet) length that

minimizes the Rényi entropy of the considered TFR [38,32]. Regarding the determination of the threshold γ, a small γ is clearly favored to avoid some data associated with the signal to be removed.

As far as mode retrieval is concerned, a critical issue is the computation of the estimation φ_k of the IF of mode k, used in (8) and carried out by *ridge extraction*, performed by fitting smooth curves with the locations of the highest energy coefficients of the considered STFT. This is usually done by considering the non-convex variational problem, whose optimal solution can be approximated using stochastic sampling or heuristic techniques [39,12,19]. This difficult problem somehow reduces the scope of the theoretical results, since the latter assumes that the ridge information is known.

5.2. Influence of frequency resolution

We here discuss the influence of the frequency resolution on FSST. Indeed, assume f is with finite length, typically defined on the interval $[0, T]$, discretized into $f(\frac{nT}{N})_{n=0,\cdots,N-1}$, and g supported on $[-\frac{LT}{N}, \frac{LT}{N}]$, with $L < N/2$, the STFT of f is then computed as follows:

$$V_f^g(t,\xi) = \int_{-\frac{LT}{N}}^{\frac{LT}{N}} f(t+\tau)g(\tau)\,\mathrm{e}^{-2\pi\mathrm{i}\tau\xi}\,\mathrm{d}\tau \approx \frac{T}{N}\sum_{n=-L}^{L} f(t+\frac{nT}{N})g(\frac{nT}{N})\,\mathrm{e}^{-2\pi\mathrm{i}\frac{nT}{N}\xi} \tag{22}$$

from which we infer that, for $0 \le p \le N-1$:

$$V_f^g(\frac{qT}{N}, \frac{pN}{MT}) \approx \frac{T}{N}\sum_{n=-L}^{L} f(\frac{(q+n)T}{N})g(\frac{nT}{N})\,\mathrm{e}^{-2\pi\mathrm{i}\frac{np}{M}}$$

for some $M \ge 2L+1$. The last sum is computed by means of a discrete FT, and the frequency resolution equals $\frac{N}{MT}$, which has the consequence that the TFR associated with FSST is all the more compact that the frequency resolution is low.

6. Mode reconstruction for strong modulations

In this section, we are interested in assessing the quality of mode reconstruction given by formula of type (8), when $d = 0$ and for different frequency resolutions, to clearly state the importance of the latter in mode reconstruction based on FSST2 evaluated on the ridge. Furthermore, we explain how FSSTs can be used in a demodulation algorithm for the purpose of mode reconstruction, the principle of which is recalled hereafter and whose performances are then compared to FSST2.

6.1. Demodulation algorithm based on FSST for mode reconstruction

We briefly recall how FSST (or FSST2) was combined in [32] with a demodulation algorithm for the purpose of mode reconstruction. Assume that for $f(t) = \sum_{k=1}^{K} A_k(t)\,\mathrm{e}^{2i\pi\phi_k(t)}$, one has computed, from FSST (or FSST2), K estimates $(\varphi_k(t))_{k=1,\cdots,K}$ of the IFs of the modes. Then, associated with each of these estimates, one defines K demodulation operators $\mathrm{e}^{-2\pi\mathrm{i}(\int_0^t \varphi_k(x)\,\mathrm{d}x-\varphi_0 t)}$, in which φ_0 is some positive constant frequency. One then remarks that, if $\varphi_k(t)$ is a good IF estimate for mode k, the signal $f_{D,k}(t) = f(t)\,\mathrm{e}^{-2\pi\mathrm{i}(\int_0^t \varphi_k(x)\,\mathrm{d}x-\varphi_0 t)}$ should contain an almost purely harmonic component at frequency φ_0, so that computing FSST for $f_{D,k}$ and then extracting the information contained in the vicinity of frequency φ_0, one can recover f_k through

$$f_k(t) \approx \left(\int_{|\omega-\varphi_0(t)|<d} T_{f_{D,k}}^{\gamma}(t,\omega)\,\mathrm{d}\omega\right)\mathrm{e}^{2\pi\mathrm{i}(\int_0^t \varphi_k(x)\,\mathrm{d}x-\varphi_0 t)} \tag{23}$$

In [32], $(\varphi_k(t))_{k=1,\cdots,K}$ were estimated as the piecewise constant curves associated with the ridges extracted from FSST (or FSST2), and were therefore greatly dependent on the frequency resolution M. We propose here a much more relevant technique to compute IFs estimates than the one based on crude ridge extraction and which will prove to be only slightly dependent on the frequency resolution. Indeed, while performing FSST (or FSST2), one computes $\widehat{\omega}_f(t,\xi)$ (or $\widehat{\omega}_f^{[2]}(t,\xi)$), which, evaluated on the ridge associated with the kth mode, i.e. $\widehat{\omega}_f(t,\varphi_k(t))$ (or $\widehat{\omega}_f^{[2]}(t,\varphi_k(t))$), leads to a much smoother IF estimate than the one proposed in [32]. This is due to the fact that the former is not constrained by the frequency resolution. In what follows, we denote, for the sake of simplicity, $\widehat{\omega}_f(t,\varphi_k(t))$ (or $\widehat{\omega}_f^{[2]}(t,\varphi_k(t))$) by $\varphi_k(t)$, depending on the studied cases.

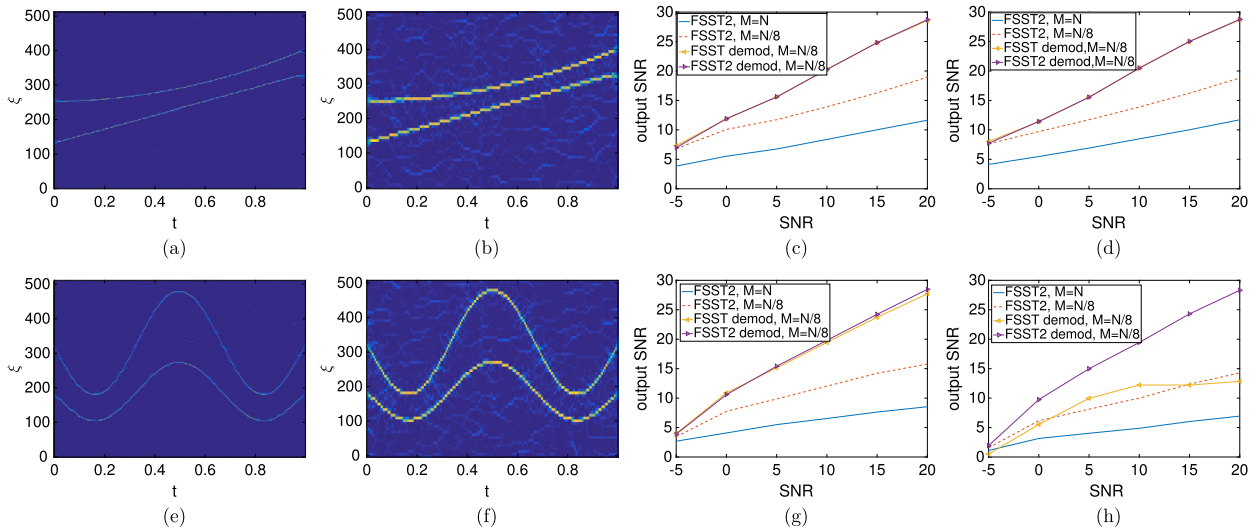

Fig. 4. (a) FSST2 of the two-chirps signal when $M = N$ (N being the signal length); (b) same as (a) when $M = N/8$; (c) reconstruction results for mode f_1 using FSST2 or the demodulation algorithm based on FSST2 or FSST (with $d = 0$, for different input SNRs, and when $f(t)$ is the two chirp signal); (d) same as (c) but for mode f_2; (e) FSST2 of the two modes with cosine phase when $M = N$, (f) same as (e) but when $M = N/8$, (g) reconstruction results for mode f_1 using FSST2 or the demodulation algorithm based on FSST2 or FSST (with $d = 0$, for different input SNR, and $f(t)$ is the signal made with two modes with cosine phase); (h) Same as (g) but for mode f_2.

6.2. Performance of the demodulation algorithm based on FSST, comparison with FSST2

We here consider two types of signal to illustrate the benefits of the demodulation procedure based on FSST (or FSST2) introduced in the previous section: the first tested signal is $f(t) = f_1(t) + f_2(t)$ made of the linear chirp $f_1(t) = 2\,\mathrm{e}^{2\pi\mathrm{i}(130t+100t^2)}$ and the quadratic chirp $f_2(t) = 2\,\mathrm{e}^{2\pi\mathrm{i}(250t+50t^3)}$, for $t \in [0, 1]$ sampled at $N = 1024$ Hz. The STFT is computed with the same L^1-normalized Gaussian window as previously, for which the optimal σ leads to a filter length $2L + 1 = 123$. The representations of the FSST2 of these signals when $M = N$ and $M = N/8 = 128$ are displayed in Figs. 4 (a) and (b), when the input SNR equals 10 dB. Then in Figs. 4 (c) and (d), we display the reconstruction results associated with modes f_1 and f_2, respectively, when $d = 0$ (meaning we only consider the information on the ridge). We either consider the direct reconstruction based on FSST2 displayed in (a) and (b) to show that a more concentrated representation results in a better reconstruction from the information on the ridge. Furthermore, we remark that using FSST or FSST2 in the demodulation process (with $M = N/8$ in the definition of STFT) does not make any difference for that type of modes (these cases are denoted by "FSST demod" and "FSST2 demod" in the considered figures) and that the results obtained with these latter techniques are significantly better than those obtained using FSST2 only. As a second illustration, we consider the signal $f(t) = f_1(t) + f_2(t)$, in which the modes have cosine phases, namely $f_1(t) = 2\,\mathrm{e}^{2\pi\mathrm{i}(190t+9\cos(3\pi t))}$ and $f_2(t) = 2\,\mathrm{e}^{2\pi\mathrm{i}(330t+16\cos(3\pi t))}$. As previously, t belongs to $[0, 1]$, $N = 1024$, and the window g remains the same (the optimal σ given by the Rényi entropy being very similar in both cases). The FSST2 of this signal computed with $M = N$ or $M = N/8$ are displayed in Figs. 4 (e) and (f), respectively. Then, we again investigate the quality of the reconstruction process, assuming $d = 0$ and when either reconstruction from FSST2 is considered or the demodulation process based on either FSST or FSST2. As in the previous case, the demodulation algorithm based on FSST2 still behaves better than FSST2 alone, as reported in Figs. 4 (g) and (h). Furthermore, we remark that while using FSST or FSST2 to compute the demodulation operator does not make any difference for mode f_1 (Fig. 4 (g)), for the more modulated mode f_2, taking into account the modulation in the demodulation operator by means of FSST2 leads to much better results (Fig. 4 (h)). To conclude, this pleads in favor of using demodulation based on FSST2 to reconstruct the modes rather than FSST2 only.

7. Conclusion and perspectives

The synchrosqueezing transform enters now its mature age, and has proven to be useful when analyzing a wide range of real-life signals. Many variants have been proposed to extend its domain of application, but open questions still remain.

(i) It is still not clear whether SST is the perfect tool for mode decomposition. The main reason is that the latter highly depends on the ridge estimation step, which is a difficult task: extracting the ridges associated with the modes from the reassigned transform seems to be a better option than doing the same thing on STFTs, but some theoretical developments still need to be carried out on that matter [40]. Furthermore, SST when used for mode reconstruction cannot operate on a STFT downsampled in time, which is a strong constraint when one has to deal with long, high-rate signals.

To circumvent this last limitation, further works are therefore needed, and, in this regard, the comparison of the results obtained with SST and alternative representations in the context of audio source separation is a first step [41].

(ii) SST suffers from the intrinsic limitation that it operates on a linear TFR, associated with a fixed TF resolution given by a global window or wavelets. This can be mitigated by using multi-taper methods [24], though there is still a lack of flexibility. More critically, any technique based on linear TFR requires TF separation for the components, which is not the case in many applications. Some recent works considered interfering or even crossing components [42], but with limited generality.

These limitations of SST make some researchers question the usefulness of SST [43], but in that paper the analysis was restricted to the original SST and the numerical investigations were carried out on simple slightly modulated modes. We definitely think that recent extensions of SST brought about two strong and clear contributions:

- the kind of results shown in [12,20], by using local slow-variation and separation assumptions, can be easily extended to other adaptive decompositions based on STFT or wavelets;
- the local instantaneous frequency and its extensions based on higher-order phase derivatives are perfectly adapted for defining a meaningful instantaneous frequency for real-life signals. Furthermore, this quantity also enables fast and accurate post-processing operations, such as ridge detection, reassignment, and mode retrieval.

References

[1] S. Mallat, A Wavelet Tour of Signal Processing, Third Edition: The Sparse Way, 3rd edition, Academic Press, 2008.
[2] A. Grossmann, J. Morlet, Decomposition of hardy functions into square integrable wavelets of constant shape, SIAM J. Math. Anal. 15 (4) (1984) 723–736.
[3] P. Flandrin, Time-Frequency/Time-Scale Analysis, vol. 10, Academic Press, 1998.
[4] K. Kodera, R. Gendrin, C. Villedary, Analysis of time-varying signals with small bt values, IEEE Trans. Acoust. Speech Signal Process. 26 (1978) 64–76.
[5] F. Auger, P. Flandrin, Improving the readability of time–frequency and time-scale representations by the reassignment method, IEEE Trans. Signal Process. 43 (5) (1995) 1068–1089.
[6] N.E. Huang, Z. Shen, S.R. Long, M.C. Wu, H.H. Shih, Q. Zheng, N.-C. Yen, C.C. Tung, H.H. Liu, The empirical mode decomposition and the Hilbert spectrum for nonlinear and non-stationary time series analysis, Proc. R. Soc. Lond., Ser. A, Math. Phys. Eng. Sci. 454 (1971) (1998) 903–995.
[7] P. Flandrin, G. Rilling, P. Goncalves, Empirical mode decomposition as a filter bank, IEEE Signal Process. Lett. 11 (2) (2004) 112–114.
[8] J. Gilles, Empirical wavelet transform, IEEE Trans. Signal Process. 61 (16) (2013) 3999–4010.
[9] M. Kowalski, A. Meynard, H. tieng Wu, Convex optimization approach to signals with fast varying instantaneous frequency, Appl. Comput. Harmon. Anal. 44 (2018) 89–122.
[10] N. Pustelnik, P. Borgnat, P. Flandrin, Empirical mode decomposition revisited by multicomponent non-smooth convex optimization, Signal Process. 102 (2014) 313–331.
[11] I. Daubechies, S. Maes, A nonlinear squeezing of the continuous wavelet transform based on auditory nerve models, in: Wavelets in Medicine and Biology, 1996, pp. 527–546.
[12] I. Daubechies, J. Lu, H.-T. Wu, Synchrosqueezed wavelet transforms: an empirical mode decomposition-like tool, Appl. Comput. Harmon. Anal. 30 (2) (2011) 243–261.
[13] M. Costa, A.A. Priplata, L.A. Lipsitz, Z. Wu, N.E. Huang, A.L. Goldberger, C.-K. Peng, Noise and poise: enhancement of postural complexity in the elderly with a stochastic-resonance-based therapy, Europhys. Lett. 77 (2007) 68008.
[14] D.A. Cummings, R.A. Irizarry, N.E. Huang, T.P. Endy, A. Nisalak, K. Ungchusak, D.S. Burke, Travelling waves in the occurrence of dengue haemorrhagic fever in Thailand, Nature 427 (2004) 344–347.
[15] Y.-Y. Lin, H-t. Wu, C.-A. Hsu, P.-C. Huang, Y.-H. Huang, Y.-L. Lo, Sleep apnea detection based on thoracic and abdominal movement signals of wearable piezoelectric bands, IEEE J. Biomed. Health Inform. 21 (6) (2017) 1533–1545.
[16] C.L. Herry, M. Frasch, A.J. Seely, H.-T. Wu, Heart beat classification from single-lead ecg using the synchrosqueezing transform, Physiol. Meas. 38 (2) (2017) 171–187.
[17] G. Thakur, H.-T. Wu, Synchrosqueezing-based recovery of instantaneous frequency from nonuniform samples, SIAM J. Math. Anal. 43 (5) (2011) 2078–2095.
[18] H.-T. Wu, Adaptive Analysis of Complex Data Sets, PhD thesis, Princeton, NJ, USA, 2011.
[19] F. Auger, P. Flandrin, Y.-T. Lin, S. McLaughlin, S. Meignen, T. Oberlin, H.-T. Wu, Time-frequency reassignment and synchrosqueezing: an overview, IEEE Signal Process. Mag. 30 (6) (2013) 32–41.
[20] T. Oberlin, S. Meignen, V. Perrier, The Fourier-based synchrosqueezing transform, in: 2014 IEEE International Conference on Acoustics, Speech and Signal Processing (ICASSP), 2014, pp. 315–319.
[21] M. Unser, D. Sage, D. Van De Ville, Multiresolution monogenic signal analysis using the Riesz–Laplace wavelet transform, IEEE Trans. Image Process. 18 (11) (2009) 2402–2418.
[22] M. Clausel, T. Oberlin, V. Perrier, The monogenic synchrosqueezed wavelet transform: a tool for the decomposition/demodulation of am-fm images, Appl. Comput. Harmon. Anal. 39 (2015) 450–486.
[23] A. Ahrabian, D. Looney, L. Stanković, D.P. Mandic, Synchrosqueezing-based time–frequency analysis of multivariate data, Signal Process. 106 (2015) 331–341.
[24] I. Daubechies, Y.G. Wang, H.-T. Wu, Conceft: concentration of frequency and time via a multitapered synchrosqueezed transform, Philos. Trans. R. Soc. A, Math. Phys. Eng. Sci. 374 (2016).
[25] H.-T. Wu, Instantaneous frequency and wave shape functions (i), Appl. Comput. Harmon. Anal. 35 (2013) 181–199.
[26] M. Skolnik, Radar Handbook, McGraw-Hill Education, 2008.
[27] J.W. Pitton, L.E. Atlas, P.J. Loughlin, Applications of positive time–frequency distributions to speech processing, IEEE Trans. Speech Audio Process. 2 (4) (1994) 554–566.
[28] E.J. Candes, P.R. Charlton, H. Helgason, Detecting highly oscillatory signals by chirplet path pursuit, Appl. Comput. Harmon. Anal. 24 (1) (2008) 14–40.
[29] B.P. Abbott, R. Abbott, T. Abbott, M. Abernathy, F. Acernese, K. Ackley, C. Adams, T. Adams, P. Addesso, R. Adhikari, et al., Observation of gravitational waves from a binary black hole merger, Phys. Rev. Lett. 116 (6) (2016) 061102.
[30] H.T. Wu, Y.W. Liu, Analyzing transient-evoked otoacoustic emissions by concentration of frequency and time, J. Acoust. Soc. Am. 144 (1) (2018) 448–466.

[31] R. Behera, S. Meignen, T. Oberlin, Theoretical analysis of the second-order synchrosqueezing transform, Appl. Comput. Harmon. Anal. 45 (2018) 379–404.
[32] S. Meignen, D.-H. Pham, S. McLaughlin, On demodulation, ridge detection and synchrosqueezing for multicomponent signals, IEEE Trans. Signal Process. 65 (8) (2017) 2093–2103.
[33] D.-H. Pham, S. Meignen, High-order synchrosqueezing transform for multicomponent signals analysis – with an application to gravitational-wave signal, IEEE Trans. Signal Process. 65 (2017) 3168–3178.
[34] T. Oberlin, S. Meignen, V. Perrier, Second-order synchrosqueezing transform or invertible reassignment? Towards ideal time–frequency representations, IEEE Trans. Signal Process. 63 (2015) 1335–1344.
[35] T. Oberlin, S. Meignen, The second-order wavelet synchrosqueezing transform, in: Proc. 42th International Conference on Acoustics, Speech, and Signal Processing (ICASSP), New Orleans, LA, USA, 5–9 March 2017.
[36] L. Stanković, A measure of some time–frequency distributions concentration, Signal Process. 81 (3) (2001) 621–631.
[37] B.P. Abbott, R. Abbott, et al., GW151226: observation of gravitational waves from a 22-solar-mass binary black hole coalescence, Phys. Rev. Lett. 116 (24) (2016) 241103.
[38] R.G. Baraniuk, P. Flandrin, A.J. Janssen, O.J. Michel, Measuring time–frequency information content using the rényi entropies, IEEE Trans. Inf. Theory 47 (4) (2001) 1391–1409.
[39] R. Carmona, W. Hwang, B. Torresani, Characterization of signals by the ridges of their wavelet transforms, IEEE Trans. Signal Process. 45 (1997) 2586–2590.
[40] S. Meignen, T. Oberlin, P. Depalle, P. Flandrin, S. McLaughlin, Adaptive multimode signal reconstruction from time–frequency representations, Philos. Trans. R. Soc. A 374 (2065) (2016) 20150205.
[41] D. Fourer, G. Peeters, Fast and adaptive blind audio source separation using recursive Levenberg-Marquardt synchrosqueezing, in: Proc. IEEE International Conference on Acoustics, Speech and Signal Processing (ICASSP), Calgary, Canada, 15–20 April 2018, pp. 766–770.
[42] V. Bruni, M. Tartaglione, D. Vitulano, On the time–frequency reassignment of interfering modes in multicomponent fm signals, in: Proc. 26th European Signal Processing Conference (EUSIPCO), Rome, 3–7 September 2018, pp. 722–726.
[43] D. Iatsenko, P.V. McClintock, A. Stefanovska, Linear and synchrosqueezed time–frequency representations revisited: overview, standards of use, resolution, reconstruction, concentration, and algorithms, Digital Signal Processing 42 (2015) 1–26.